Localization microscopy for the study of amyloid fibril formation

Dorothea Pinotsi[a], Gabriele S. Kaminski Schierle[a], Eric Rees [a], Clemens F. Kaminski[a];
[a]Department of Chemical Engineering and Biotechnology, University of Cambridge, Cambridge

ABSTRACT

Super-resolution microscopy has emerged as a powerful and non-invasive tool for the study of molecular processes both *in vitro*, but also as they occur in live cells. Here we present the application of *direct* stochastic optical reconstruction microscopy (*d*STORM), a super-resolution technique based on single molecule localization, to determine the morphology of protein aggregates and of small extra- and intracellular structures. The technique reveals details down to 20 nm providing information on scales much smaller than the wavelength of the probing light. We use *d*STORM in the study of amyloid fibril self-assembly processes associated with neurodegenerative diseases, such as Alzheimer's and Parkinson's diseases. We show that the aggregation process can be followed kinetically and observe the emergence of amyloid structures in time as they occur *in vitro*. As an all optical technique, there is translation potential from studies *in vitro* to *in vivo* applications.

Keywords: super-resolution microscopy, amyloid fibrils, in situ imaging

1. INTRODUCTION

Understanding the fundamental mechanisms behind the formation of highly organized aggregate structures from originally soluble proteins is one of the key challenges of current biophysical and life science research. Proteins are the fundamental building blocks of living systems, exhibiting a wide range of biological functions for which their folding into functional conformational states is essential. Failure in this mechanism, so called protein misfolding, can lead them to subsequent aggregation with potential toxic effects to cells or organisms [1]. Misfolding and aggregation are related to a number of increasingly prevalent pathological conditions, including neurodegenerative diseases such as Alzheimer's (AD) and Parkinson's (PD) disease. At the heart of these diseases are so called intrinsically disordered proteins which occur naturally in the brain and which in their native, soluble state, are usually harmless. Their misfolding however leads to formation of insoluble aggregates, so-called amyloid fibrils, causing neuronal cells to malfunction, and eventually leading to severe injury and death of neurons. The fibrillar states of different amyloid proteins are remarkably similar with respect to their structure and morphology: they are composed of several protofilaments of highly ordered β-sheet rich structures, twisted around a common axis to form long fibrils with diameters typically in the 2 to 15 nm range and lengths that can reach up to several microns [2]. However, the precise nature of their toxic gain of function is not currently understood.

In order to investigate the molecular mechanisms of aggregation and to relate the emergence of aggregates with toxic effects, novel biophysical techniques are required capable of a direct visualization of the misfolding and aggregation process in biologically relevant model systems. To obtain reproducible data on structural transformations and correlations with *in vivo* toxicity is extremely challenging but is of immense relevance in the search for pathways of therapeutic intervention, e.g. in drug discovery for aggregation inhibiting compounds. While mature amyloid fibrils have been extensively studied by electron microscopy (EM), NMR, and X-ray diffraction, these techniques can only be performed *ex situ* and have no capability to track the kinetics of amyloid self-assembly from the formation of small oligomers to the development of full-length fibrils. Fluorescence based biophysical assays have proven to be valuable in this context. Providing *kinetic* information on the aggregation process, e.g. *via* the increase in intrinsic or extrinsic fluorescence of aggregates, during their formation, in labeled [3], [4], or label-free assays [5], [6] or by monitoring indirectly the formation of aggregating species in live cells [7], [8]. However, the *in vitro* assays are based on ensemble measurements, which do not provide any detailed insight into the individual processes. Hence, there is a compelling need for new methods to monitor the dynamics of the amyloid aggregation process directly and non-invasively, which share the advantages of fluorescence techniques but offer the resolution advantages of *ex situ* biophysical techniques such as

Nanoimaging and Nanospectroscopy, edited by Prabhat Verma,
Alexander Egner, Proc. of SPIE Vol. 8815, 88150G · © 2013 SPIE
CCC code: 0277-786X/13/$18 · doi: 10.1117/12.2022589

EM. Here we report on the use of optical super-resolution microscopy techniques [9], [10], [11], [12] to bridge this gap. In particular we show that *direct* stochastic optical reconstruction microscopy (*d*STORM) [12] offers unprecedented insights into the complex process of amyloid fibril self-assembly, at nanometer resolution.

We thus apply this technique in order to quantify protein aggregation reactions both *in vitro* and in cells. We particularly focus on visualizing the structure and growth mechanisms of α-synuclein fibrils. Aggregation of α-synuclein, a small, natively unfolded protein, is linked to Parkinson's disease. To this end, we used α-synuclein protein with covalently attached fluorescent dyes which produced labeled fibrils. We give guidelines on how to extract meaningful quantitative data from localization microscopy data in the context of amyloid research and validate this using a correlative AFM/*d*STORM imaging. We then apply this approach in order to study differences in the morphology of species formed in cells and in the test tube. We also reveal information on the uptake of small aggregates by cells and follow their structural fate: these points are particularly important in the context of biomedical research into the molecular origins of amyloid mediated neurodegenerative diseases. Finally, further studies are currently undertaken in order to study the kinetics and the molecular mechanisms taking place during the aggregation of this protein, by monitoring the addition of monomers to pre-existing fibrils (seeds), with two-color *d*STORM.

2. MATERIALS AND METHODS

2.1 Protein labeling

Monomeric α-synuclein protein was labeled in the following way: the residue 122, at the C-terminal end was selected as a position for incorporating the fluorophores. This residue is located outside the region thought to form the fibrillar structure (the so called NAC region) [13] and thus there are no influences in the kinetics and ensuing structures of forming aggregates through the addition of the fluorophores, as this was independently confirmed by AFM, EM and ThT kinetic assays [4].

The N-122C mutant variant of α-synuclein was labeled with either maleimide-modified Alexa Fluor 647 or Alexa Fluor 568 dyes (Invitrogen, Carlsbad, CA, USA) via the cysteine thiol moiety [14]. The labeled protein was purified from the excess of free dye by a P10 desalting column with Sephadex G25 matrix (GE Healthcare, Waukesha, WI, USA), divided into aliquots, flash frozen, and stored at −80°C. Each aliquot was thawed immediately and used only once. The efficiency of the labeling process was determined by mass spectrometry (Mass spectrometry facility, Department of Biochemistry, University of Cambridge), resulting to be higher than 95% for Alexa Fluor 647 and 50% for Alexa Fluor 568.

2.2 Conversion of monomeric protein to fibrils

Human α-synuclein was incubated at 800 μM (in 20 mM phosphate buffer at pH 7.4) for 50 h at 45°C under strong stirring with a Teflon coated stir bar.

Fibrillar seeds of α-synuclein at 80 μM were produced according to two protocols: in the first one, the fibrils formed were diluted to 80 μM with PBS buffer and sonicated 10 sec with a probe sonicator (Bandelin, Solopuls HD 2070), using 10% maximum power and 30% cycles, yielding fibril lengths of approximately 200 nm. In the second case the fibrils were not sonicated but only stirred overnight, yielding variable lengths of approximately 400 nm. All seeds were labeled at a 1:20 ratio with Alexa Fluor 568 or with Alexa Fluor 647. The seeds were subsequently incubated with labeled monomeric protein at 10fold higher concentration. The monomeric α-synuclein was labeled at a 1:20 ratio with Alexa Fluor 568 or 647. The incubation at 37°C took place in an Eppendorf tube and samples at the end of the reaction were removed for subsequent imaging with microscopy techniques.

2.3 Super-resolution fluorescence microscopy by single molecule localization and *d*STORM imaging

Super-resolution imaging was performed with a *d*STORM microscopy setup, based on a Nikon Eclipse TE 300 inverted widefield microscope, and a 100x, 1.49 NA TIRF objective lens (Nikon UK Ltd.). The setup is described in detail in [15], [16]. Samples were placed on a glass or quartz coverslip glued at the bottom of an imaging chamber.

Photoswitching buffer solution was added, which consisted of 100 mM mercaptoethylamine (MEA) in phosphate buffered saline (PBS, pH 7.4), together with a glucose-enzyme oxygen scavenger (40 mg/ml glucose, 5μg/ml glucose oxidase, 1 μg/ml catalase). The chamber was filled to the top and sealed with a glass coverslip to minimize entrance of oxygen. Laser illumination was at 640 nm (Toptica Photonic AG, Graefelfing, Germany) for excitation of the Alexa 647 dye and at 561 nm (Oxxius SLIM-561) for excitation of the Alexa 568 dye. Laser beams were collimated and combined by dichroic mirrors and a beam expanding telescope. They were subsequently focused onto the back focal plane of the objective. A 405 nm (120 mW) (Mitsubishi Electronics Corp., Tokyo, Japan), laser was used as reactivation source. The fluorescence light in the detection path went through a dichroic filter (Semrock multi-edge filter Di01-R405/488/561/635-25x36 followed by a FF01-446/523/600/677-25 filter, Semrock, Rochester NY, USA) and was subsequently filtered further using band-pass filters (Semrock BP-607/35-25 and BP-642/35-25) for the fluorescence from the 647 and the 568 dye respectively, before being projected on a low-noise, highly sensitive electron-multiplying CCD camera (Ixon DV887 ECS-BV, Andor). The excitation intensity was 2 kW/cm^2 for the Toptica laser and 5 kW/cm^2 for the Oxxius laser. The reactivation laser was only turned on when the number of active fluorophores in the field of view was reduced, and no spatial drift of the sample was observed during the acquisition time. Imaging was performed in TIRF (total internal reflection microscopy) or under highly inclined (HI) illumination conditions [17] to reduce out of focus background signal and improve signal to noise ratios. The former leads to the illumination of the sample in a layer extending ca.100 nm above the cover slip. With HI illumination it is possible to image deeper into the region above the coverslip (ca. 5 μm). The area imaged was 64x64 pixels corresponding to an area on the sample of ~10x10 μm^2.

Typically, 10.000-20.000 fluorescence frames with 10-12 msec exposure time were recorded; the exposure time was matched with the "on" state of the fluorescent dyes. From each image stack a reconstructed *d*STORM image was generated by using in-house developed software [18] based on MATLAB (The MathWork Inc., Natick, USA).

2.4 Super-resolution algorithm for localization and visualization

To obtain super-resolved images of the specimens, the raw image data were processed using mainly the Open Source rainSTORM localization microscopy software [18] and for validation also using the rapidSTORM software package [19]. The rainSTORM analysis and visualization was as follows: fluorophore positions were determined by applying a "sparse segmentation and least squares Gaussian fitting" algorithm to the data [20]. Imprecise localizations were excluded by a one-parameter quality-control technique: localizations were rejected if their localization precision, estimated using the Thompson formula [21], was worse than a user-defined threshold. The accepted localizations were visualized using an Adaptive Gaussian Rendering method: this is a method of Adaptive Kernel Density Estimation [30], in which each localization is plotted in the reconstructed image as a Gaussian "kernel" of fluorescence density. The width of each kernel is suitably chosen based upon the Thompson Precision estimate of the corresponding localization, as well as the density of observed localizations, so that the final reconstructed image is the best possible match to the true fluorescence density of the specimen [18]. The match between the reconstruction and the true density of the specimen is optimized subject to a few assumptions, particularly: (a) that the Thompson precision estimates are approximately correct and not spoiled by inaccurate background fluorescence estimation, and hence that the reconstruction is rendered using kernels of optimized width, and (b) that artifacts arising from "false positive" mislocalizations are well-excluded by the quality control criterion.

2.5 Image Analysis

Data image analysis was performed using ImageJ (NIH, Bethesda, Maryland, USA) to determine fibril cross sections, and our rainSTORM software to quantify corresponding localization microscopy parameters such as localization precision and visualization kernel width within the cross section region. It is noted that the true fluorescence density of the specimen is blurred by (only) two steps in a localization microscopy experiment [18]: first by convolution with the Localization Spread function, and second by convolution with the kernel used to visualize the reconstructed image. Provided some assumptions hold, the true fibril width can be deconvolved from the width of the fibril in the reconstructed image. Essentially, the reconstructed image generated from a sufficiently large number of localizations is obtained by convolving the true fluorescence density with two approximately Gaussian blurring functions. These describe (a) the localization error, and (b) the visualization smoothing. Therefore, if we assume that the fibril cross section is Gaussian with a thickness that corresponds to a standard deviation of d, then the observed thickness W is related to the localization precision σ and visualization kernel size h by Equation 1:

$$d^2 = W^2 - (\sigma^2 + h^2) \qquad [1]$$

The observed cross section (W) of a fibril can be determined by analyzing a super-resolution image generated using the Gaussian rendering method of Section 2.4 (namely by analysis of a few hundred cross sections in ImageJ). The corresponding σ values can be determined from the average Thompson precision estimate of the relevant localizations. The corresponding average kernel width (h) is determined in the reconstruction algorithm (in practice h is negligibly small in the case of plentiful localizations). Thus, the true fibril width d can be determined using the approximate deconvolution of Equation 1.

2.6 Correlative AFM imaging

Atomic Force Microscopy (AFM) was used in order to obtain correlative information on the structure of the grown fibrils imaged with super-resolution microscopy. Correlative AFM/*d*STORM imaging on the same fibrils was achieved by using nano-patterned quartz slides, with gold alignment markers. The alignment markers were fabricated using electron beam lithography and gold deposition. This type of correlative AFM imaging has been previously used in [22].

AFM images were acquired using a VEECO Dimension 3100 atomic force microscope (Bruker AXS, Cambridge, UK). The instrument was operated in tapping mode in air using silicon cantilevers with a resonant frequency of 300 kHz, a spring constant of 40 N/m and a tip radius of 10 nm (RTESP, Bruker AXS, Cambridge, UK).

Images were collected at a scan rate of 1 Hz. In standard AFM imaging, 5 μL of each fibrillar sample was deposited onto freshly cleaved mica surfaces for 2 hours for adsorption. The samples were rinsed with 200 μL of Milli-Q water 5 times and left to dry completely in air before imaging.

For the correlative imaging on quartz: First, the sample was imaged using *d*STORM in TIRF mode. The quartz slide was glued at the bottom of a well with Silicon glue (Exaktosil N15 silicone duplicating material A & B, Bredent, UK) that could be removed upon drying. Photoswitching buffer was added in the well to enable imaging with *d*STORM. The fibril positions on the markers grid were noted. Subsequently, the quartz slide, with the fibrils adsorbed onto the surface, was removed from the well, cleaned with DI water and dried using a nitrogen gun. After cleaning, the quartz slide was transferred to the AFM and the aggregate structures at the same locations as before were found and imaged in tapping mode.

2.7 Cell culture

SH-SY5Y human neuroblastoma cells were obtained from LGC standards (Teddington, UK). Cells are maintained on 1:1 minimal essential medium (MEM; Sigma, Gillingham, UK) : nutrient mixture F12 Ham (Sigma), 15% foetal bovine serum (Life technologies, Paisley, UK), 1% L-glutamine (Sigma), 1% MEM non-essential amino acids (Sigma) and 1% antibiotic-antimycotic (10,000 U penicillin, 10,000 μg streptomycin, 25 μg amphotericin B, Life technologies). All incubations with α-synuclein were carried out by replacing the foetal bovine serum with 2% B27 complement (Life technologies). All incubations of fibrils in cell cultures were performed at 8 μM final concentration of seed fibrils labeled with Alexa 568 (1:20 labeled:unlabeled ratio), in a Lab-Tek II chambered coverslip glass. After 1 and after 24 hours of incubation the cells were washed and fixed for imaging with *d*STORM.

3. RESULTS AND DISCUSSION

3.1 Imaging of amyloid fibrils with *d*STORM in vitro

Recently, localization microscopy has been used in different studies in order to probe the morphology of protein aggregates *in vitro*, but also *in situ*, in cells. This has empowered studies of aggregation related diseases. In particular, *d*STORM was used to image the aggregate morphologies of Aβ with a resolution better than 20 nm [16]. Super-resolution microcopy was also used to visualize Huntingtin aggregates [22], [23] and α-synuclein amyloid fibrils [24], [25].

For the current study of α-synuclein aggregation and structure we used monomeric protein with covalently attached fluorescent dyes which produced labeled fibrils (see Materials and Methods for details on fibril preparation). Direct labeling of α-synuclein is advantageous in order to probe the morphology of the aggregates, as compared to immunofluorescence staining, because of the small size of the fluorescent dye which is directly attached to the protein peptide sequence.

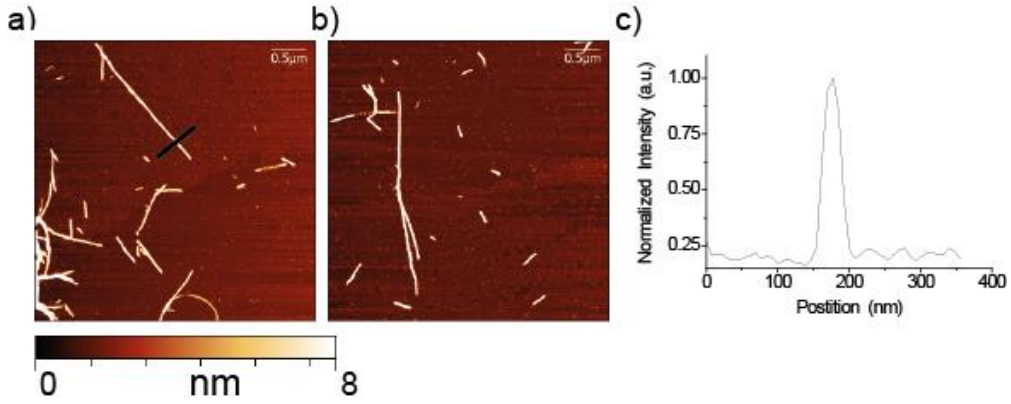

Figure 1: a) and b) AFM images of covalently labeled α-synuclein amyloid fibrils with Alexa Fluor 647, in an area containing different sized fibrils. c) Normalized intensity cross section profile for the black line depicted in a). A mean diameter of 23.4 +/- 1.8 nm was found after analyzing several of these AFM images (including tip convolution).

AFM images of these structures are depicted in Figure 1 a) and b), showing the morphology of the fibrils. The mean value of the measured fibril widths was 23.4 +/- 1.8 nm and the mean height corresponded to 9 nm. The measured fibril width includes the AFM tip convolution whereas the height corresponds more accurately to the true fibril diameter. Through *d*STORM we obtained high resolution images of the labeled amyloid fibrils, as depicted in Figure 2.

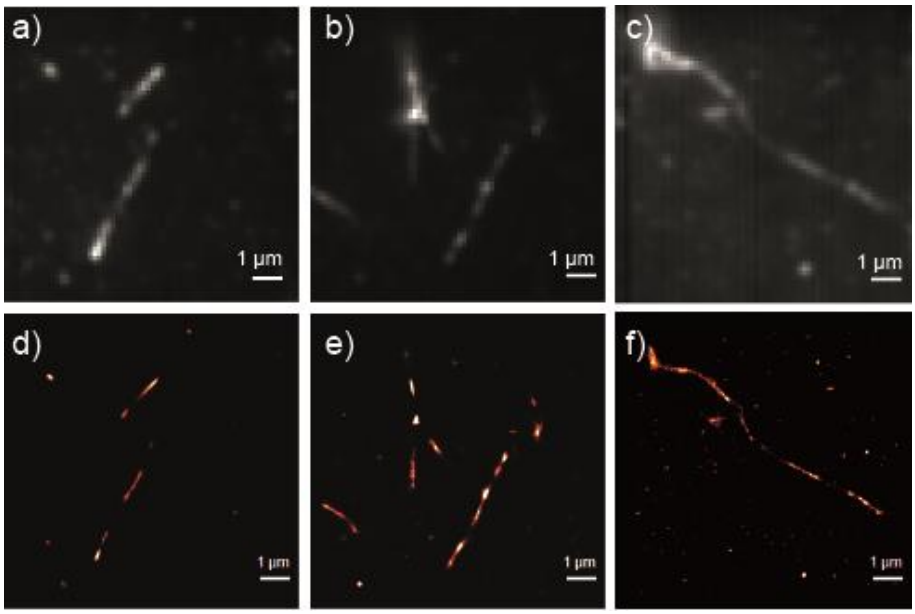

Figure 2: Super-resolution images of directly labeled α-synuclein amyloid fibrils with Alexa Fluor 647. a), b) and c) Conventional (diffraction limited) fluorescence images of the fibrils. d), e) and f) Corresponding *d*STORM images.

Figure 2 shows the corresponding *d*STORM images of fibrils labeled with Alexa Fluor 647. They have been produced by incubation of fibrillar seeds with monomeric protein, as described in the Materials and Methods section. Fig. 2 a), b) and c) show the conventional fluorescence and diffraction limited images of the fibrils. In Fig. 2 d), e) and f) the corresponding super-resolved images are displayed. Further studies are currently performed to image the amyloid structures at each point of the aggregation process, which informs on the growth process at the single fibril level.

3.2 Analysis of amyloid fibril thickness

Using the method described in Sections 2.4 and 2.5 we performed a detailed analysis of the fibril widths based on our *d*STORM data. An example is shown for the two fibrils depicted in Figure 2d). Using ImageJ we took the average of 50 cross sections for each of the two fibrils individually, A and B as shown in Figure 3a) and b). This gave the values for the observed fibril width of 90 and 87 nm for the cross-sections A and B respectively. Thus the standard deviation of these observed distributions was equal to $W = FWHM_{meas} / 2\sqrt{2\ln(2)}$ where $FWHM_{meas}$ is the measured fibril thickness in ImageJ. Given the corresponding average Thompson precisions and the known values of *h* used for the reconstructed images, using Equation (1) we get a standard deviation *d*, or a true fibril width of 13.2 nm and 8.7 nm for A and B fibril cross sections, respectively. The results are consistent with values obtained from the literature and with the ones obtained with AFM. We note that this method is more accurate than simply taking the cross-section of the reconstructed image of the fibril, since it accounts for any significant localization error. However, for the extracted values to be precise the following condition should be fulfilled: $\sigma < d$, which means that the localization precision should be smaller than the true fibril diameter. This is a challenging goal for the experiment (given the small fibril diameters), nevertheless the present analysis is valuable in order to quantify the required precision that would allow for an accurate measurement of fibril diameters.

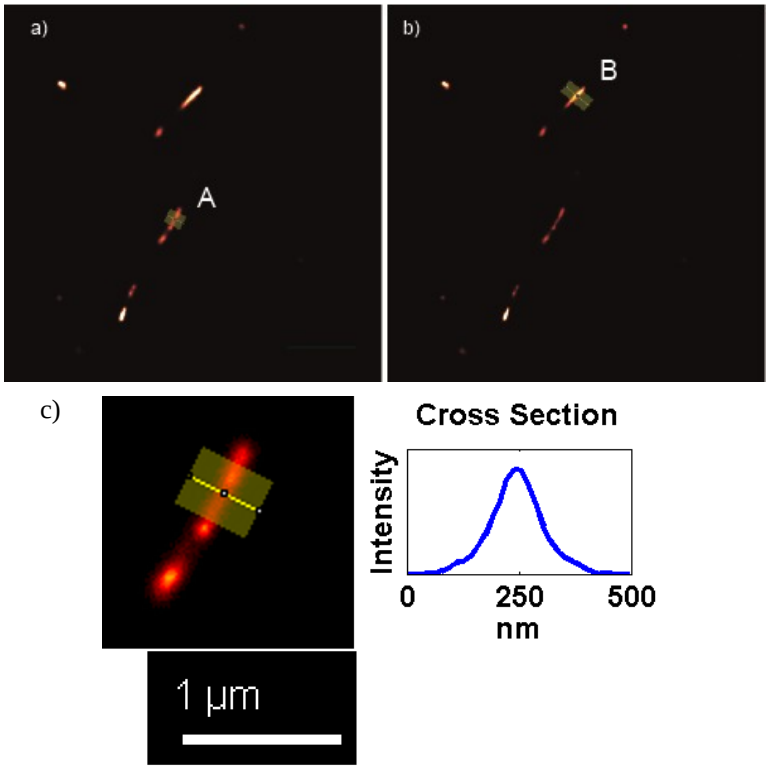

Figure 3: a), b) Super-resolution images of directly labeled α-synuclein amyloid fibrils with Alexa Fluor 647. The areas corresponding to the cross sections examined are depicted. c) Zoom in into one fibril and plot showing the intensity profile of the cross section, yielding the fibril width.

3.3 Correlative AFM/*d*STORM

In order to correlate the morphology of AFM images with the fluorescence super-resolved results we performed AFM and *d*STORM in conjunction, on the same amyloid fibrils. We produced amyloid fibrils labeled with Alexa 647 and using quartz slides with nano-fabricated markers (see Materials and Methods for details), we were able to image the exact same fibrils with AFM and *d*STORM. Quartz is atomically flat (as mica) and is hence suitable for AFM imaging. The gold grid deposited on the cover slips as described earlier, contained markers to help in the location of protein fibrils with both microscopy techniques. The *d*STORM imaging was performed first and the quartz slide was then transferred to the AFM instrument as described in Materials and Methods.

Figure 4 shows two examples of amyloid fibrils imaged with correlative AFM/*d*STORM. Fig. 4a) and d) show the AFM image of the fibrils, Fig. 4b) and e) depict the corresponding *d*STORM images and finally Fig. 4c) and f) display the overlay images of the previous techniques.

We note that not all the fibrils visible by AFM are seen in the *d*STORM channel. This is likely due to several reasons: 1) in the experiment performed in TIRF illumination, only the fibrils that are already adsorbed on the quartz surface are imaged. As the experiment proceeds however, more and more fibrils are deposited on the quartz surface *via* sedimentation. These fibrils are thus not present/visible via TIRF and *d*STORM imaging, but do appear during later investigation by AFM. 2) During the transfer time between the two microscope setups and the sample preparation (washing and drying the quartz coverslip), it is likely that fibrils that are not well adsorbed onto the surface are changing location. Thus, even though they were not at the specific locations during the *d*STORM imaging, they appear in the AFM images. 3) Fibrils which are out of focus in the TIRF experiment, or less bright are not included in the super-resolved image, since they produce inaccurate localizations and are thus rejected by the reconstruction/visualization algorithm. However, these fibrils can be imaged with the AFM. 4) Finally, smaller aggregates are less likely to be imaged by both

techniques, as they are less strongly adsorbed to the quartz coverslip and they are prone to move or detach/desorb during the transfer and washing steps. Despite these issues, the correlative AFM/*d*STORM technique can be powerful in determining accurately the morphology of a single fibril.

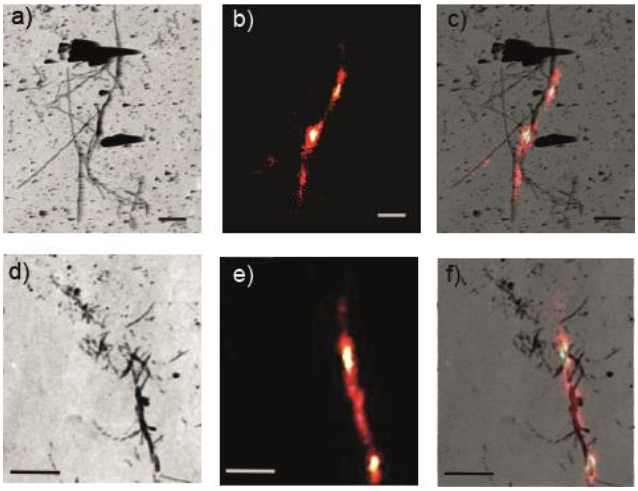

Figure 4: Correlative AFM and *d*STORM imaging of α-synuclein amyloid fibrils. a), d) AFM images of fibrils, b) and e) super-resolved images of the same fibrils, c) overlay image of the *d*STORM and the AFM images. Scale bars: 1 µm.

3.4 Imaging of amyloid fibrils in cells

Until recently it has been challenging to study aggregation with molecular level detail in cellular environments. Methods using variants of FRET or homoFRET [4], [7], [26] are powerful to follow aggregation dynamics in cells, however they are indirect methods and do not *per se* offer morphological detail on ensuing amyloid states [7]. Super-resolution microscopy can address this challenge however, and we have pioneered the use of *d*STORM imaging in the context of aggregate imaging in cells [27], [28]. We used *d*STORM to investigate questions relating to the trafficking and transmission of amyloid fibrils into, and between, cells in order to obtain information of molecular mechanisms of disease transmission. In order to answer this question, we incubated small sized fibrillar seeds (with lengths of ~500 nm) of α-synuclein labeled with Alexa Fluor 568 in the extracellular medium of human neuroblastoma differentiated cells (see Materials and Methods for details). Namely, we added 8 µM of the fibrils in the extracellular medium of the cells and let them incubate at 37°C. After 1 hour of incubation and after washing off the extracellular medium and fixing the cells, we obtained *d*STORM images of the aggregates in the cells in TIRF illumination.

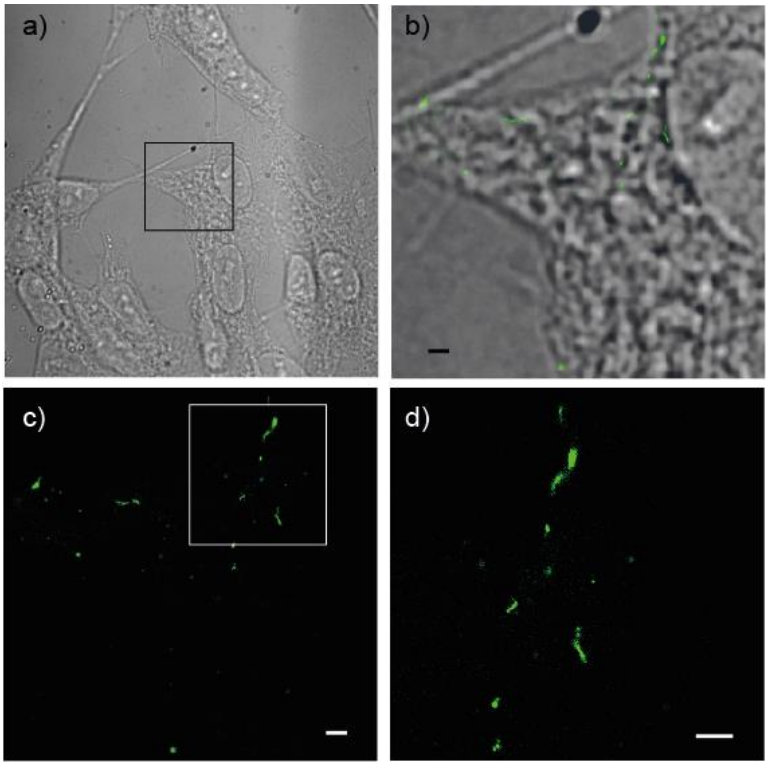

Figure 5: *d*STORM imaging of α-synuclein amyloid fibrils in cells after 1 h of incubation. a) DIC image of an area containing the human neuroblastoma cells under study, after 1 hour of incubation of fibrillar seeds in cell medium. b) Overlay of the DIC and the *d*STORM image at TIRF illumination mode to image deep at the cell membrane, zoomed in at the area enclosed by the square in a). c) *d*STORM image of only the fluorescence. d) Magnified image of the area depicted in c). Scale bars: 1 µm.

In Figure 5a) we show a DIC image of cells after one hour of incubation had passed. Fig. 5b) is an image overlay of DIC and *d*STORM data in a zoomed-in version of the area denoted by the square in Fig. 5a). Figure 5c) shows only the *d*STORM fluorescence image. These images have been obtained in TIRF mode showing that the fibrils have just entered through the cell membrane. This implies that already after 1 hour the small sized aggregates are taken up by the cells. Fig. 5d) is a magnified image of the area enclosed by the white square in Fig. 5c), showing fibrillar structures of less than 1 µm size, similar to the initial fibrils in the incubating solution. This demonstrates that no further aggregation had taken place prior to entry. This is important in the context of disease because there has been speculation that polysaccharides on the cell membrane (e.g. glycosaminoglycans) have aggregation accelerating effects [29], but our data show that no further aggregation takes place prior to entry, a result that would have not been observable with a conventional microscopy technique.

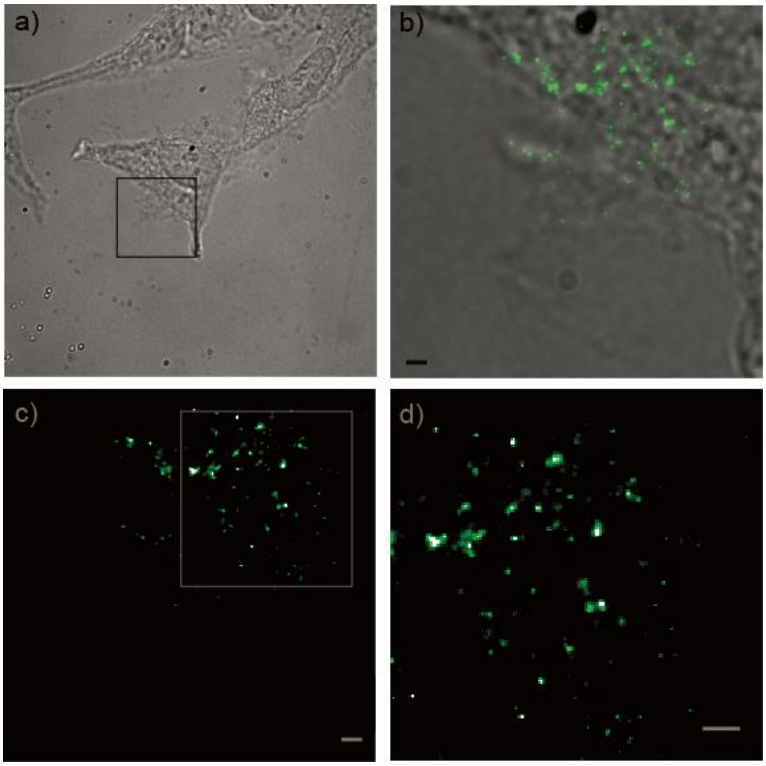

Figure 6: *d*STORM imaging of α-synuclein amyloid fibrils in cells after 24 h of incubation. a) DIC image of a cell under study, after 24 hours of incubation of fibrillar seeds in cell medium. b) Overlay of the DIC and the *d*STORM image in highly inclined illumination mode to image deep inside the cell, zoomed in at the area enclosed by the square in a). c) *d*STORM image of only the fluorescence. d) Magnified image of the area depicted in c). Scale bars: 1 µm.

After 24 hours of incubation, a marked difference is observable in the type and quantity of species taken up by the cells In Fig 6a) and b) DIC and DIC/*d*STORM overlays are shown respectively clearly pointing to the existence of much larger aggregates inside the cell. Images from the *d*STORM channel are depicted in Fig. 6c) and 6d), this time obtained using the highly inclined illumination mode, to permit imaging deeper into the cells. Clearly fibrils have aggregated further inside the cells, but the structures differ in morphology compared to what was observed *in vitro* (Fig. 2). Instead of the linear aggregates seen to form *in vitro*, the aggregates in the cells adopt a tightly packed, mostly spherical structure. We hypothesize that the fibrillar seeds are packaged into endo- or lysosomes and that 1) they either form bigger clusters once inside these structures or, 2) that endogenous monomeric α-synuclein protein cross reacts with the species entering from the outside, and that aggregation of endogenous monomeric protein is seeded by entry of exogenous species. These phenomena are not possible to be observed currently by any other biophysical techniques, demonstrating the power of super-resolution imaging in the field. Further studies are currently under way to elucidate the differences between the aggregation dynamics observed *in vitro* versus those occurring in cells.

4. CONCLUSIONS

In the present work we applied single molecule localization super-resolution microscopy in order to study the formation of protein aggregates and fibrillar structures, associated with neurodegenerative diseases, and elucidated important differences in the phenomena that occur *in vitro* and in cells. We show that it is possible to obtain high resolution structural information of amyloid fibrils, which are covalently labeled, offering advantages in specificity, patho-physiological relevance, and image resolution compared to previously used techniques requiring antibody labels. We presented a quantitative method to extract true fibril diameters from our *d*STORM data showing that resolution

enhancements are obtained compared to previous reports with antibody labeled moieties, which suffer due to the size of the antibody structure, which is significant in comparison to the fibril diameters. We also quantified the required localization precision in order to accurately determine these challenging small values. We validated the developed techniques using a correlative imaging approach combining AFM and *d*STORM measurements on fibrils formed *in vitro*. Finally, we present the application of *d*STORM imaging *in situ*. We are able to observe the entry of small aggregated species into cells, and the subsequent growth into globular, highly compact aggregates once inside cells, which show marked differences to the morphology shown in the *in vitro* case. The results demonstrate that advanced optical imaging techniques are powerful methods to elucidate the molecular mechanisms of amyloid formation, and trafficking in the context of neurodegenerative diseases.

ACKNOWLEDGEMENTS

This work was funded by grants from the Medical Research Council UK (MR/K015850/1), the Alzheimer Research UK Trust (ARUK-EG2012A-1), the EPSRC (EP/H018301/1) and the Wellcome Trust (089703/Z/09/Z). D.P. wishes to acknowledge support from the Swiss National Science Foundation through a personal fellowship. We thank Alexander Buell for useful discussions and Celine Galvagnion for the expression of and help with the labeling of α-synuclein.

REFERENCES

[1] C. M. Dobson, "Protein folding and misfolding.," *Nature*, vol. 426, no. 6968, pp. 884–90, Dec. 2003.

[2] A. W. P. Fitzpatrick, G. T. Debelouchina, M. J. Bayro, D. K. Clare, M. A. Caporini, V. S. Bajaj, C. P. Jaroniec, L. Wang, V. Ladizhansky, S. A. Müller, C. E. MacPhee, C. A. Waudby, H. R. Mott, A. De Simone, T. P. J. Knowles, H. R. Saibil, M. Vendruscolo, E. V Orlova, R. G. Griffin, and C. M. Dobson, "Atomic structure and hierarchical assembly of a cross-β amyloid fibril.," *Proceedings of the National Academy of Sciences of the United States of America*, vol. 110, no. 14, pp. 5468–73, Apr. 2013.

[3] E. Hellstrand, B. Boland, D. M. Walsh, and S. Linse, "Amyloid β-Protein Aggregation Produces Highly Reproducible Kinetic Data and Occurs by a Two-Phase Process.," *ACS chemical neuroscience*, vol. 1, no. 1, pp. 13–8, Jan. 2010.

[4] T. J. van Ham, A. Esposito, J. R. Kumita, S.-T. D. Hsu, G. S. Kaminski Schierle, C. F. Kaminski, C. M. Dobson, E. A. A. Nollen, and C. W. Bertoncini, "Towards multiparametric fluorescent imaging of amyloid formation: studies of a YFP model of alpha-synuclein aggregation.," *Journal of molecular biology*, vol. 395, no. 3, pp. 627–42, Jan. 2010.

[5] D. Pinotsi, A. K. Buell, C. M. Dobson, G. S. Kaminski Schierle, and C. F. Kaminski, "A label-free, quantitative assay of amyloid fibril growth based on intrinsic fluorescence.," *Chembiochem : a European journal of chemical biology*, vol. 14, no. 7, pp. 846–50, May 2013.

[6] F. T. S. Chan, G. S. Kaminski Schierle, J. R. Kumita, C. W. Bertoncini, C. M. Dobson, and C. F. Kaminski, "Protein amyloids develop an intrinsic fluorescence signature during aggregation.," *The Analyst*, vol. 138, no. 7, pp. 2156–62, Apr. 2013.

[7] G. S. Kaminski Schierle, C. W. Bertoncini, F. T. S. Chan, A. T. van der Goot, S. Schwedler, J. Skepper, S. Schlachter, T. van Ham, A. Esposito, J. R. Kumita, E. A. A. Nollen, C. M. Dobson, and C. F. Kaminski, "A FRET sensor for non-invasive imaging of amyloid formation in vivo.," *Chemphyschem : a European journal of chemical physics and physical chemistry*, vol. 12, no. 3, pp. 673–80, Feb. 2011.

[8] T. Murakami, S.-P. Yang, L. Xie, T. Kawano, D. Fu, A. Mukai, C. Bohm, F. Chen, J. Robertson, H. Suzuki, G. G. Tartaglia, M. Vendruscolo, G. S. Kaminski Schierle, F. T. S. Chan, A. Moloney, D. Crowther, C. F. Kaminski, M. Zhen, and P. St George-Hyslop, "ALS mutations in FUS cause neuronal dysfunction and death in Caenorhabditis elegans by a dominant gain-of-function mechanism.," *Human molecular genetics*, vol. 21, no. 1, pp. 1–9, Jan. 2012.

[9] E. Betzig, G. H. Patterson, R. Sougrat, O. W. Lindwasser, S. Olenych, J. S. Bonifacino, M. W. Davidson, J. Lippincott-Schwartz, and H. F. Hess, "Imaging intracellular fluorescent proteins at nanometer resolution.," *Science (New York, N.Y.)*, vol. 313, no. 5793, pp. 1642–5, Sep. 2006.

[10] S. W. Hell and J. Wichmann, "Breaking the diffraction resolution limit by stimulated emission: stimulated-emission-depletion fluorescence microscopy," *Optics Letters*, vol. 19, no. 11, p. 780, Jun. 1994.

[11] S. T. Hess, T. P. K. Girirajan, and M. D. Mason, "Ultra-high resolution imaging by fluorescence photoactivation localization microscopy.," *Biophysical journal*, vol. 91, no. 11, pp. 4258–72, Dec. 2006.

[12] M. Heilemann, S. van de Linde, M. Schüttpelz, R. Kasper, B. Seefeldt, A. Mukherjee, P. Tinnefeld, and M. Sauer, "Subdiffraction-resolution fluorescence imaging with conventional fluorescent probes.," *Angewandte Chemie (International ed. in English)*, vol. 47, no. 33, pp. 6172–6, Jan. 2008.

[13] H. Heise, W. Hoyer, S. Becker, O. C. Andronesi, D. Riedel, and M. Baldus, "Molecular-level secondary structure, polymorphism, and dynamics of full-length alpha-synuclein fibrils studied by solid-state NMR.," *Proceedings of the National Academy of Sciences of the United States of America*, vol. 102, no. 44, pp. 15871–6, Nov. 2005.

[14] S. Thirunavukkuarasu, E. A. Jares-Erijman, and T. M. Jovin, "Multiparametric fluorescence detection of early stages in the amyloid protein aggregation of pyrene-labeled alpha-synuclein.," *Journal of molecular biology*, vol. 378, no. 5, pp. 1064–73, May 2008.

[15] M. Erdelyi, E. Rees, D. Metcalf, G. S. K. Schierle, L. Dudas, J. Sinko, A. E. Knight, and C. F. Kaminski, "Correcting chromatic offset in multicolor super-resolution localization microscopy," *Optics Express*, vol. 21, no. 9, p. 10978, Apr. 2013.

[16] G. S. Kaminski Schierle, S. van de Linde, M. Erdelyi, E. K. Esbjörner, T. Klein, E. Rees, C. W. Bertoncini, C. M. Dobson, M. Sauer, and C. F. Kaminski, "In situ measurements of the formation and morphology of intracellular β-amyloid fibrils by super-resolution fluorescence imaging.," *Journal of the American Chemical Society*, vol. 133, no. 33, pp. 12902–5, Aug. 2011.

[17] M. Tokunaga, N. Imamoto, and K. Sakata-Sogawa, "Highly inclined thin illumination enables clear single-molecule imaging in cells.," *Nature methods*, vol. 5, no. 2, pp. 159–61, Mar. 2008.

[18] E. J. Rees, M. Erdelyi, D. Pinotsi, A. Knight, D. Metcalf, and C. F. Kaminski, "Blind assessment of localisation microscope image resolution," *Optical Nanoscopy*, vol. 1, no. 1, p. 12, 2012.

[19] S. Wolter, A. Löschberger, T. Holm, S. Aufmkolk, M.-C. Dabauvalle, S. van de Linde, and M. Sauer, "rapidSTORM: accurate, fast open-source software for localization microscopy.," *Nature methods*, vol. 9, no. 11, pp. 1040–1, Nov. 2012.

[20] S. Wolter, M. Schüttpelz, M. Tscherepanow, S. VAN DE Linde, M. Heilemann, and M. Sauer, "Real-time computation of subdiffraction-resolution fluorescence images.," *Journal of microscopy*, vol. 237, no. 1, pp. 12–22, Jan. 2010.

[21] R. E. Thompson, D. R. Larson, and W. W. Webb, “Precise nanometer localization analysis for individual fluorescent probes.,” *Biophysical journal*, vol. 82, no. 5, pp. 2775–83, May 2002.

[22] W. C. Duim, B. Chen, J. Frydman, and W. E. Moerner, “Sub-Diffraction Imaging of Huntingtin Protein Aggregates by Fluorescence Blink-Microscopy and Atomic Force Microscopy.,” *Chemphyschem : a European journal of chemical physics and physical chemistry*, vol. 12, pp. 2387 – 2390, Jul. 2011.

[23] S. J. Sahl, L. E. Weiss, W. C. Duim, J. Frydman, and W. E. Moerner, “Cellular inclusion bodies of mutant huntingtin exon 1 obscure small fibrillar aggregate species.,” *Scientific reports*, vol. 2, p. 895, Jan. 2012.

[24] M. J. Roberti, J. Fölling, M. S. Celej, M. Bossi, T. M. Jovin, and E. a Jares-Erijman, “Imaging nanometer-sized α-synuclein aggregates by superresolution fluorescence localization microscopy.,” *Biophysical journal*, vol. 102, no. 7, pp. 1598–607, Apr. 2012.

[25] J. Ries, V. Udayar, A. Soragni, S. Hornemann, K. P. R. Nilsson, R. Riek, C. Hock, H. Ewers, A. a Aguzzi, and L. Rajendran, “Superresolution Imaging of Amyloid Fibrils with Binding-Activated Probes.,” *ACS chemical neuroscience*, Apr. 2013.

[26] F. T. S. Chan, C. F. Kaminski, and G. S. Kaminski Schierle, “HomoFRET fluorescence anisotropy imaging as a tool to study molecular self-assembly in live cells.,” *Chemphyschem : a European journal of chemical physics and physical chemistry*, vol. 12, no. 3, pp. 500–9, Feb. 2011.

[27] G. S. K. Schierle, S. Van De Linde, M. Erdelyi, E. K. Esbj, T. Klein, E. Rees, C. W. Bertoncini, C. M. Dobson, M. Sauer, and C. F. Kaminski, “In Situ Measurements of the Formation and Morphology of,” pp. 12902–12905, 2011.

[28] M. Ahn, E. De Genst, G. S. Kaminski Schierle, M. Erdelyi, C. F. Kaminski, C. M. Dobson, and J. R. Kumita, “Analysis of the native structure, stability and aggregation of biotinylated human lysozyme.,” *PloS one*, vol. 7, no. 11, p. e50192, Jan. 2012.

[29] M. Goedert, R. Jakes, M. G. Spillantini, M. Hasegawa, M. J. Smith, and R. A. Crowther, “Assembly of microtubule-associated protein tau into Alzheimer-like filaments induced by sulphated glycosaminoglycans.,” *Nature*, vol. 383, no. 6600, pp. 550–3, Oct. 1996.

[30] B.W. Silverman, ‘’Density Estimation for Statistics and Data Analysis’’, Chapman and Hall, New York (1986).